Digest Journal of Nanomaterials and Biostructures Vol. 20, No. 4, October-December 2025, p. 1223-1233

Influence of Ag doping on the structural, optical and elemental properties of CuO nanocrystals

G. Ravindra Devi Revathy [a], L. Balakrishnan [a,*], K. Swethaa [b], K. S. Pugazhvadivu [c]

[a] *Department of Physics, Government College of Technology, Coimbatore, Tamilnadu-641013, India*

[b] *Department of Physics, Government College of Engineering, Bodi, Tamilnadu-625582, India*

[c] *Department of Physics, Rajalakshmi Engineering College, Chennai, Tamilnadu-602105, India*

Copper (or cupric) oxide (CuO) is an eminent material which employs in disparate applications such as photodetectors, battery electrodes, memory devices, transistors and gas sensors. An effortless hydrothermal process was implemented to synthesis virgin CuO and CuO doped nanoparticles (NPs). Detailed investigation was carried out to analyze the ensue of doping of Ag within CuO NPs. The impact of Ag doping on structural, optical, morphological and elemental characteristics were analyzed using X-ray diffractometer (XRD), UV-Vis diffuse reflectance spectrometer (UV-Vis DRS), photoluminescence spectrometer (PL), field-emission scanning electron microscope (FESEM), energy dispersive spectrometer (EDAX) and X-ray photoelectron spectrometer (XPS). XRD confirmed the material's crystalline nature by displaying the diffracted pattern of monoclinic phased CuO and the average crystallite size computed through Cauchy Lorentzian equation found to increase on Ag doping. The high absorbance and low reflectance of pristine and Ag doped CuO NPs obtained from UV-Vis DRS facilitates the material to well suit for visible photodetection application. The PL reveals the information about the defects and recombination efficiency of the material. The agglomerated flaky nature of the samples was determined through FESEM. The ratio of elements was analyzed through EDAX. The XPS survey spectrum confirmed the appearance of all required constituents of sample and core level spectrum illustrated their chemical states.

(Received June 12, 2025; Accepted October 8, 2025)

Keywords: CuO, Nanoparticle, Ag doped CuO, Doping, Hydrothermal

1. Introduction

Copper oxide nanoparticles (CuO NPs), a class of transition metal oxide nanomaterials, have garnered significant recognition ascribed to their specific structural, electrical, optical, catalytic and elemental properties. CuO NPs primarily exists in two stable oxidation states: cuprous (or di-copper) oxide (Cu_2O), which possess crystal structure with cubic phase and copper (or cupric) oxide (CuO), which adopts monoclinic structure. A huge variety of techniques has been employed to achieve the CuO NPs synthesis with diverse morphologies, including thermal oxidation [1], solution [2], hydrolysis [3], template-based sol–gel [4] and electrochemical [5]. Moreover, the hydrothermal [6], solvothermal [7] and microwave-hydrothermal [8, 9] methods were widely used to tune their structural and morphological characteristics towards photodetector application. In this work, CuO NPs was doped with silver (Ag) to examine the influence of Ag on CuO via various characterization techniques in the perspective of photodetection. The previous studies mention that transition metal doping in CuO increases electron-hole separation, fine tunes the band gap and offers high sensitivity for photodetection.

The introduction of surfactants facilitates the controlled formation of CuO/Cu_2O nanostructures. Among these, CuO gained captivation owing to their limited bandgap (~1.4 eV)

* Corresponding author: bslv85@gmail.com
https://doi.org/10.15251/DJNB.2025.204.1223

[10] and excellent stability. Their remarkable properties make them highly suitable for various applications across multiple domains. In electronics and optoelectronics, CuO NPs play a crucial role in thin-film transistors, solar cells, gas sensors [11, 12], battery electrodes [13, 14], memory devices [15], field effect transistors [16] and photodetectors owing to their semiconducting nature. Recent studies have highlighted the advantages of different synthesis techniques. Bhattacharya and Mukherjee (2019) reported that the sol-gel method offers superior control over particle size and morphology, while hydrothermal synthesis enhances crystallinity [17]. Zhou et. al. (2020) further demonstrated that CuO's narrow bandgap enables efficient light absorption, making it suitable for photodetector [19, 20], photocatalytic and gas-sensing applications [18, 21]. Moreover, CuO NPs are emerging as promising materials for energy storage attributed to their large surface and favourable electrical conductivity [22]. Patel and Sharma (2022) reported their application in batteries containing lithium ions, where the charge storage capacity is enhanced, while Wang et. al. (2023) explored their potential in supercapacitors for high-power energy storage [23].

Given these promising attributes, CuO NPs are anticipated to exhibit superior qualities relative to their bulk ones with high volumes. Hydrothermal synthesis method was executed to explore and optimize the properties of CuO NPs. Also, investigated the impact of incorporation of Ag on morphological, structural, elemental and optical qualities of CuO towards visible photodetector application.

2. Materials and method

2.1. Preparation of CuO nanoparticles

The renowned method of hydrothermal was performed for the synthesis of CuO NPs. This method uses aqueous solution as solvent. Precedingly, 2.15 g of cupric nitrate (Cu $(NO_3)_2$) disintegrated in deionized (DI) water (50ml) and stirred well for half an hour. Secondly, 1.92 g of sodium hydroxide (NaOH) was solubilized in DI water (50ml) in a separate beaker and then allowed to whirl for next half an hour. Then NaOH solution is gradually mixed up with the Cu $(NO_3)_2$ solution and stirred well for another half an hour. Consequently, 1 g of Cetyltrimethylammonium bromide (CTAB) (binding agent) was dissolved in DI water (30ml) and stirred well until it gets dissolved completely. This CTAB solution is mixed with the prepared mixture and stirred altogether for about 2 h. The product obtained is poured to a Teflon container which is then placed in as autoclave made of stainless-steel. Then it is kept inside a forced air oven for 24 h at 150 °C. Afterwards, that mixture is cooled till it acquires normal room temperature. Obtained powder, which is settled at the bottom of the Teflon container is centrifuged with ethanol and DI water for multiple times to assure its purity. The perfectly washed powder is then subjected to dry at 80 °C for 10 h. Eventually, for 2 hr the dried powder is kept in muffle furnace to calcinate at 500 °C.

2.2. Synthesis of Ag doped CuO nanoparticles

The above-mentioned procedure was followed for the preparation of Ag doped CuO (CuO:Ag) NPs. Aqueous Cu $(NO_3)_2$ and NaOH is added with CTAB, 1 (atomic %) at. % of silver nitrate ($AgNO_3$) was mixed and stirred together vigorously for 2 h. The resultant mixture was autoclaved at 150 °C for 24 h. Once it attains normal room temperature, settled powder was cleansed with DI water through centrifuge method. The obtained powder was dried for 10 h at 80 °C and tempered for 2 h at 500 °C. Finally, 1 at. % Ag doped CuO (CuO:Ag 1 at. %) NPs was obtained. Accordingly, the similar methodology was adopted for the preparation of 3 at. %, 5 at. %, 7 at. % Ag doped CuO (CuO:Ag 3 at. %, 5 at. % and 7 at. %) NPs.

3. XRD analysis

The structure of crystal and phase composition of obtained CuO NPs were examined using XRD. The graph (Fig. 1) presents diffracted image of CuO:Ag NPs within 20° to 80° (2θ range).

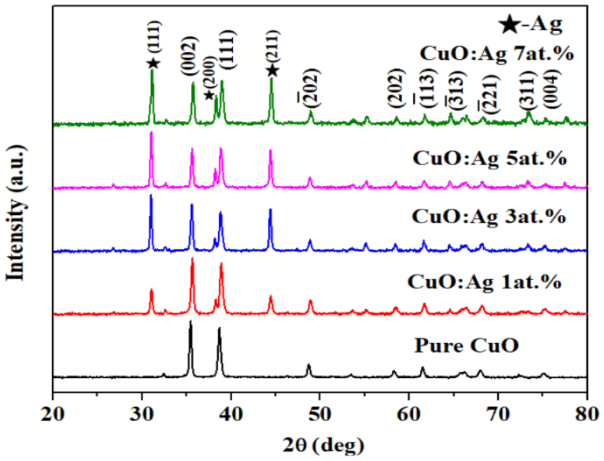

Fig. 1. XRD analysis - pure CuO and CuO:Ag nanocrystals.

For pure CuO, high-intensity diffraction peaks are noticed at 2θ values 35.3° and 38.6°, correlative with (002) and (111) crystal planes, respectively. Additional significant Bragg's reflection peaks appear at 2θ values corresponding to the crystal planes ($\bar{2}02$), (202), ($\bar{1}13$), ($\bar{3}13$), ($\bar{2}21$), (311) and (004). These peaks closely match the reference data provided in JCPDS card no 00–041-0254, confirming the identity of the CuO NPs. XRD intensity peaks further indicates the polycrystalline nature of CuO NPs with C2/c space group which exists as monoclinic crystal. XRD pattern of CuO:Ag NPs present extra peaks at positions corresponding to (111), (200) and (211) crystal planes, which are marked with star (★) in the Fig. 1. These peaks signify the formation of Ag clusters due to the presence of excess dopant atoms or the solubility limit of CuO. The analysis validates the synthesis of CuO:Ag NPs, with structural modifications induced by the presence of the dopant Ag. When CuO:Ag shows extra peaks in an XRD pattern, it usually indicates the presence of a secondary phase, likely metallic silver nanoparticles, which have formed alongside the CuO lattice due to the doping process, causing additional diffraction peaks that was not seen in pure CuO. Further investigation is required to explore the impact of Ag incorporation on physical and chemical aspects of host CuO NPs.

Table 1. The peak position (2θ) variation, full width at half maximum (FWHM, β) value, interplanar spacing (d), volume of cell (V) and average crystallite size (D) of pure CuO and CuO:Ag NPs.

Specimens	2θ (deg.)	'β' (deg.)	d (Å)	V $(Å)^3$	D (nm)
Pure CuO	35.5	0.5	2.522	81.08	50
	38.6	1.2	2.319		
CuO: Ag 1 at. %	35.7	1.6	2.510		
	38.98	1.5	2.289	94.34	36
CuO: Ag 3 at. %	35.6	2.1	2.516		
	38.9	2.2	2.294	98.57	38
CuO: Ag 5 at. %	35.6	3.6	2.516		
	38.8	3.7	2.307	104.45	30
CuO: Ag 7 at. %	35.7	4.2	2.510		
	38.98	4.7	2.289	109.97	47

Cauchy Lorentzian (eqn. (1)) method is widely used for estimating the average crystallite size [24]. By utilizing the Cauchy Lorentzian equation, researchers can gain valuable insights into the microstructural properties of materials, aiding the understanding of their physical and mechanical behaviours.

$$\beta \cos\theta = K\lambda/D + 4\varepsilon\sin\theta \quad (1)$$

Here θ is the Bragg's angle, K a constant with value 0.9, called shape factor, λ is X-ray's wavelength (λ = 0.15405 nm) and the strain is denoted by ε. Here, D is determined by analysing high-intensity peaks in the diffracted pattern. By employing this approach, Table 1 represents the estimated D values of all synthesized pristine and CuO:Ag (NPs). The effect of dopant concentration on D depends on dopant type, its ionic radius, charge and solubility into the lattice of host CuO. Here, the result illustrates that D decreased after the addition of different Ag concentrations.

4. Optical properties

The interaction of light with the synthesized nanocrystals is pivotal for understanding their optical properties. Fig. 2 illustrates the absorbance spectra of the prepared CuO:Ag nanocrystals. Fig. 2 reveals, the absorption-edge of CuO:Ag 1 at. % and CuO:Ag 3 at. % nanocrystals with a minimal increase, which was ascribed to low silver doping.

With an increase in silver doping concentration to CuO:Ag 5 at. % and 7 at. %, a noticeable shift in the absorption edge to higher intensities is observed. Despite the shift, the absorption wavelength for all CuO:Ag samples remain redshifted when compared to pure CuO nanocrystals. Fig. 3 reveals the reflectance spectra of pristine CuO and CuO:Ag nanocrystals. All CuO:Ag (especially CuO:Ag 5 at. %) samples exhibit low reflectance which accounts the better optical response relative to pure CuO and can act as efficient materials for photodetection.

The photoluminescence spectrometer (PL) was utilized to determine the recombination and defect level in pure CuO and CuO:Ag 5 at. % sample which exhibited higher absorption and low reflectance compared to other CuO:Ag samples. CuO:Ag 5 at. % with high intense absorption peak was compared with pure CuO to notedown the difference in emission. The near edge emission occurs at 359 nm wherein electrons in conduction band readily reunites with the holes in valence band. The CuO:Ag 5 at. % showed a lower recombination rate and higher oxygen

vaccancy peak centred at 380 nm compared to pure CuO which benefits a photodetector by enhancing its detection capability. The oxygen vaccancies traps the charges from the visible light thereby enhancing the photo responsivity and lower the recombination rate [24].

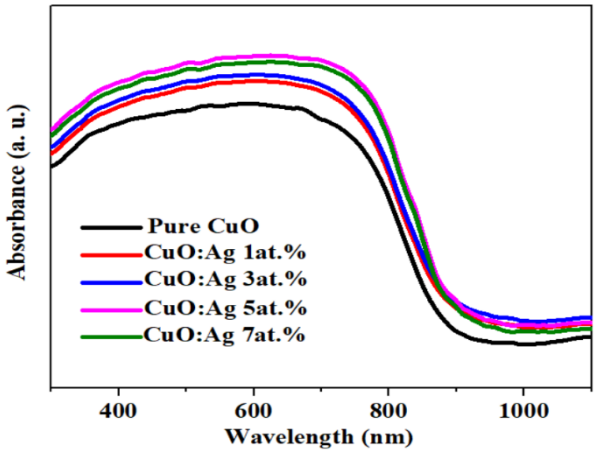

Fig. 2. Absorbance spectra of pure CuO and CuO:Ag nanocrystals between 400-1000 nm.

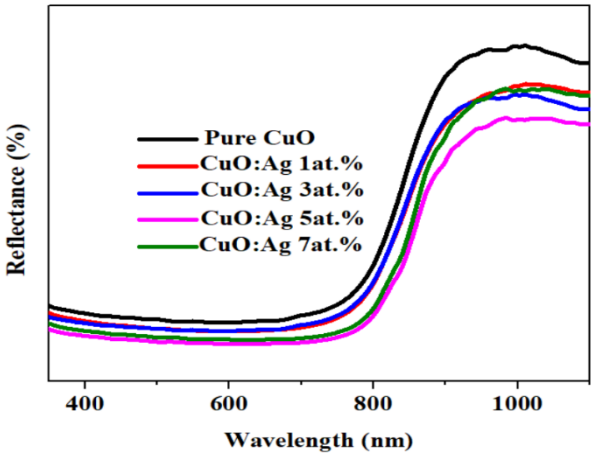

Fig. 3. Diffuse reflectance spectra of pure CuO and CuO:Ag nanocrystals between 400-1000 nm.

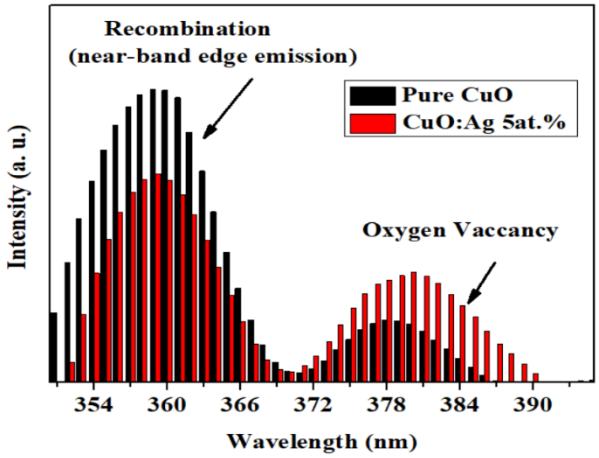

Fig. 4. PL emission spectra of pure CuO and CuO:Ag 5 at. %.

5. Surface analysis

The size distribution and topography of prepared NPs play a pivotal role in their functional properties. Fig. 5 [(a) & (b)] represents FESEM micrograph of CuO and Fig. 5 [(c) & (d)] represents CuO:Ag 5 at. % NPs which reveal distinct morphological features relative to pure CuO. The investigation provides insights into the degree of crystallinity, porosity and agglomeration, which are essential for potential applications. The images indicate the flaky porous morphology of the oxide compound formed due to the aggregation of minute nanoparticles in the nano meter range. The lattice fringes can be clearly seen in the figures, which specifies the formation of highly crystalline porous nanostructure. The CuO:Ag nanoparticles exhibit a higher degree of agglomeration, which may be attributed to strong interparticle interactions or inadequate dispersion during synthesis. This aggregation can influence the functional properties of the material by altering its surface area and reactivity. The rough surface morphology observed in these samples suggests enhanced porosity needing large surface areas, which can be highly favourable for processes like adsorption and catalysis.

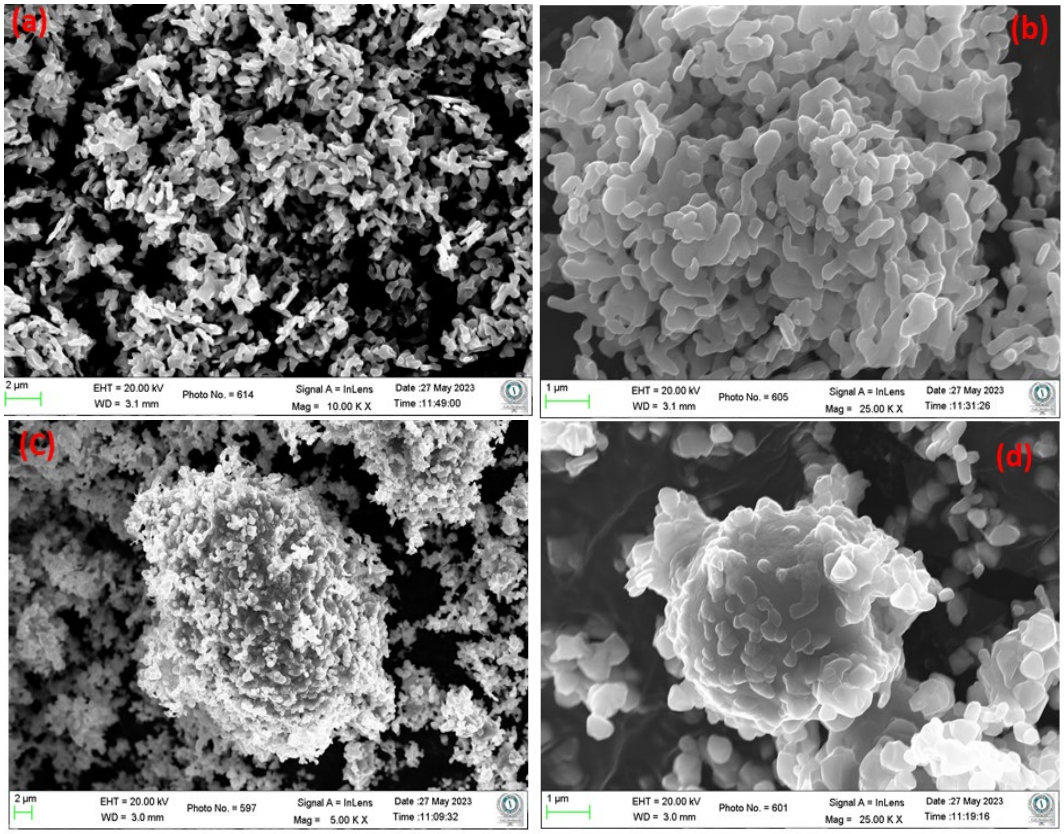

Fig. 5. FESEM image of nanocrystals (a) & (b) pure CuO; (c) & (d) CuO:Ag 5at. % at different magnifications.

6. Elemental analysis

Energy Dispersive Analysis of X-ray (EDAX) is a powerful analytical method utilized to ascertain the elemental constitution of the materials. In this analysis, EDAX was performed on as-prepared CuO (Fig. 6 [(a) and (b)]) and CuO:Ag (Fig. 6 [(c) and (d)]), providing crucial insights into their purity and composition. Table 2 lists the percentage of atoms present in the elements. The EDAX spectra reveal major peaks corresponding to copper (Cu) and oxygen (O) in pure CuO

and in CuO:Ag samples, peaks corresponding to silver (Ag) are also detected, verifying successful doping of CuO with Ag. The occurrence of high intense Cu and O peaks in the undoped CuO spectra confirms its purity, with no significant impurity elements detected. In CuO:Ag samples, the detection of Cu, O and Ag peaks further evident the successful incorporation of Ag into the CuO matrix [25].

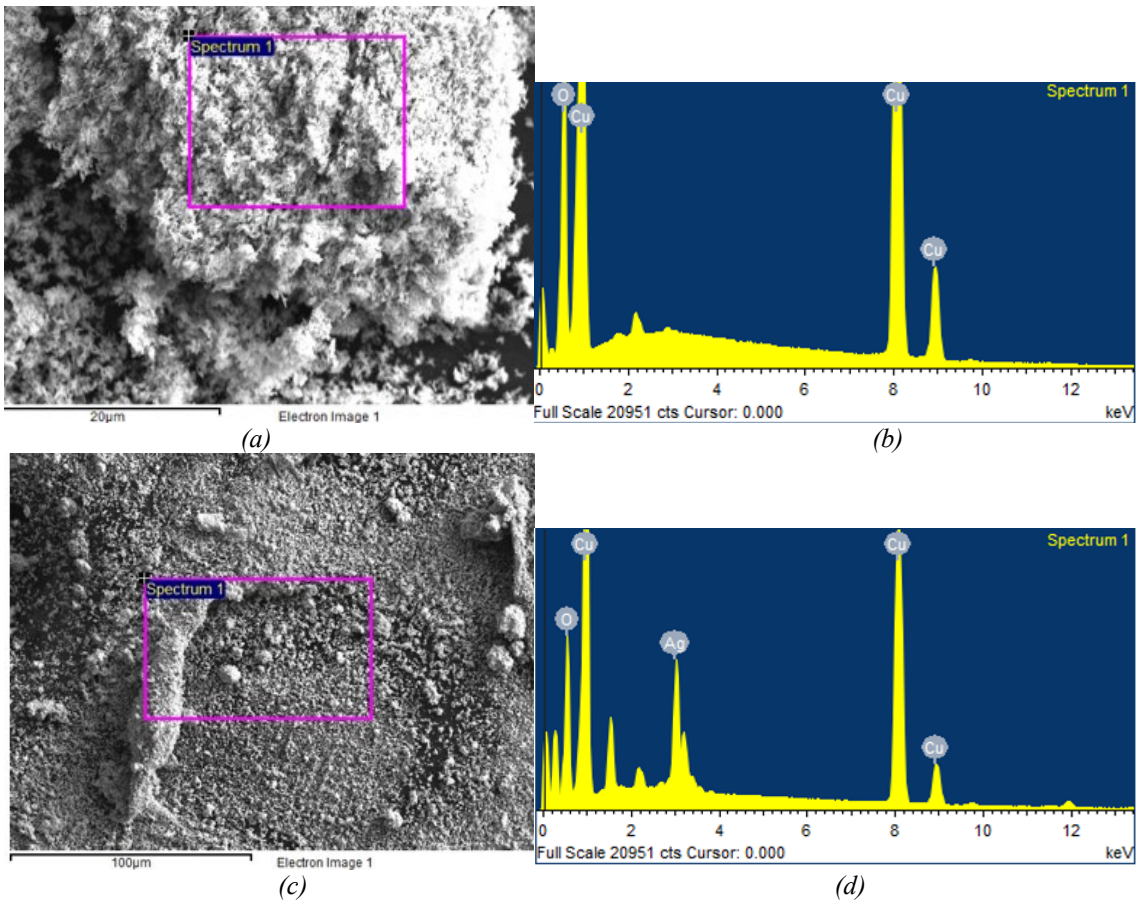

Fig. 6. (a) Microscopic picture and (b) EDAX peaks of pure CuO. (c) Microscope picture and (d) EDAX peaks of CuO:Ag 5 at. %.

Table 2. Elemental composition of CuO and CuO:Ag 5 at. % NPs.

Samples	Element	Weight%	Atomic%
CuO:Ag 5at. %	O K	21.61	53.94
	Cu K	65.94	41.45
	Ag L	12.45	4.61
	Total	100	100
CuO	O K	16.32	43.64
	Cu K	83.68	56.36
	Totals	100	100

7. XPS analysis

XPS was employed to obtain the information about binding energy, surface composition and elemental chemical states contained in CuO and CuO:Ag 5 at. %. The survey scan in Fig. 7(a) confirms the occurrence of Cu and O in CuO sample and Fig. 8(a) additionally validates the appearance of Ag in CuO:Ag 5 at. %.

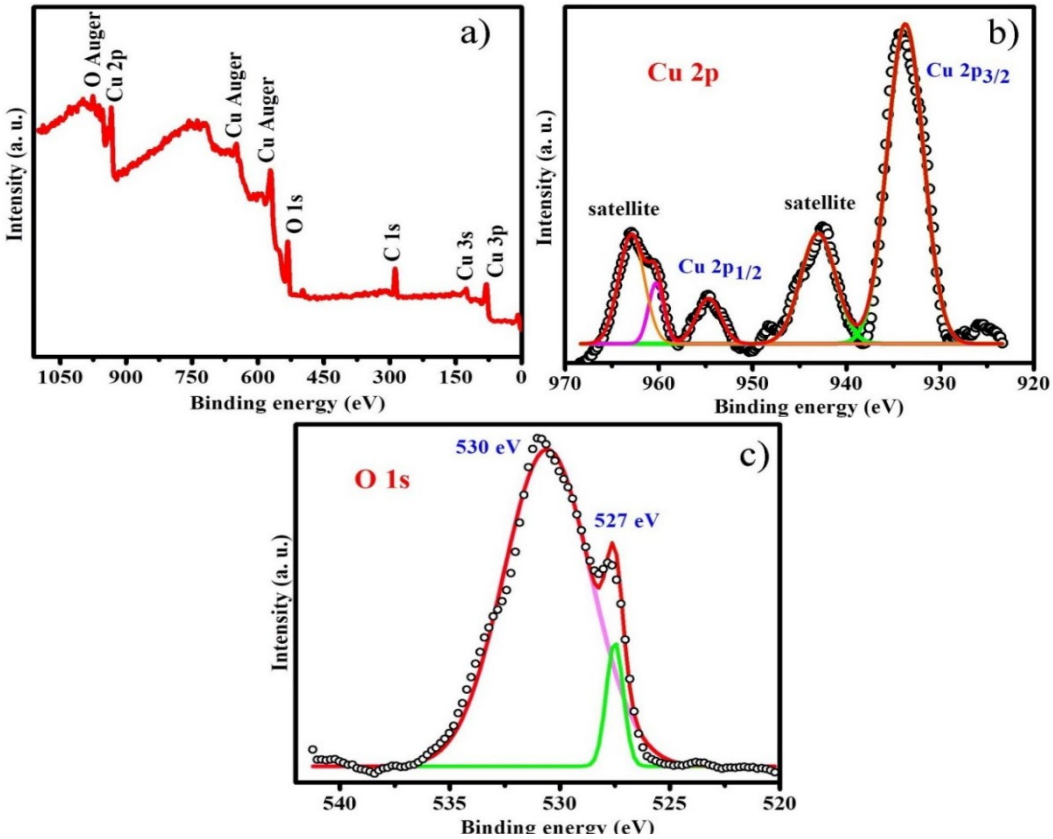

Fig. 7. (a) XPS survey spectrum of pure CuO, core level spectrum of (b) Cu 2p and (c) O 1s in pure CuO.

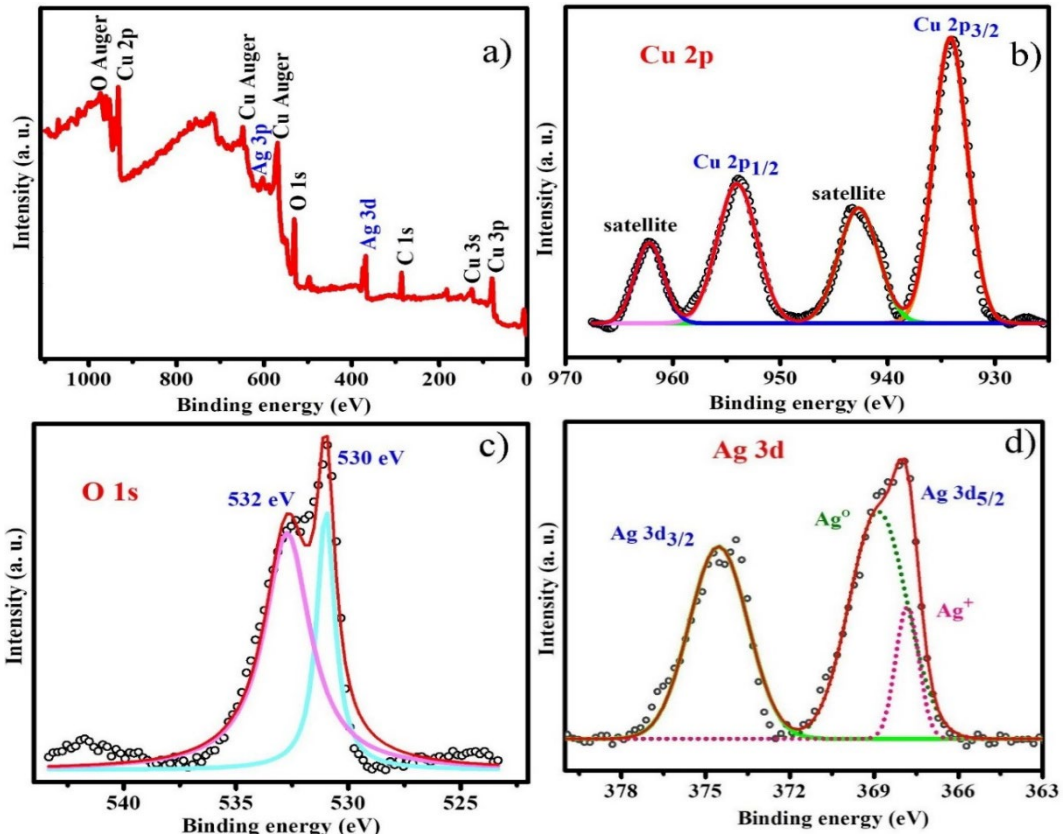

Fig. 8. (a) XPS survey spectrum of CuO:Ag 5 at. %, core level spectrum of (b) Cu 2p, (c) O 1s and (d) Ag 3d in CuO:Ag 5 at. %.

The core level spectrum (Fig. 7(b)) of Cu 2p elucidates the existence of two states, Cu $2p_{3/2}$ state with binding energy value of 933 eV and Cu $2p_{1/2}$ with 962 eV. The same case repeated in core level spectra of Cu 2p in CuO:Ag 5 at. % sample (Fig. 8(b)) indicating that doping Ag created no impact in altering the binding energy of Cu. Even more, the Cu 2p core level spectra (Figs. 7(b) and 8(b)) show two satellite (shake-up) peaks at 942 eV (Cu $2p_{3/2}$ satellite) and 954 eV (Cu $2p_{1/2}$ satellite) which were in accordance with the previous results implicit the residence of partially filled Cu $3d^9$ shell which reveals the occupancy of Cu^{2+} [26]. Fig. 7(c) displays the core level spectra of O 1s which divulge two peaks one at 527 eV due to formation of Cu-O bond ascribed to the absorption of O on Cu surface and the other at 530 eV corresponds to the hydroxyl ion absorption by the O atoms [26]. Also, CuO:Ag 5 at. % shows the presence of two O1s peaks at 530 eV (Cu absorbed O) and at 532 eV (hydroxyl absorption by O) with the increase in binding energies attributed to Ag doping. The core level spectrum (Fig. 8(d)) discloses the Ag's chemical states Ag $3d_{5/2}$ and Ag $3d_{3/2}$. The Ag $3d_{5/2}$ peak was deconvoluted into two characteristic peaks with energies 368 eV and 369 eV correspond with two different chemical state of Ag likely Ag^+ (ionic state) and Ag^0 (metallic state) respectively, whereas, Ag $3d_{3/2}$ peak centred at 374 eV [27].

8. Conclusion

The monoclinic structured pure and different concentrations of CuO:Ag were prepared by hydrothermal method. The XRD characterization confirm the formation of monoclinic structure. CuO:Ag 5 at. % shows better UV absorption and low reflectance which is favourable for the photo detection application. The low recombination rate and high oxygen vacancies of CuO:Ag 5 at. % assures high detectivity and sensitivity for photodetection. The aggregated flake morphology and the presence of all elements assured by FESEM and EDAX. The XPS survey authenticate the

residence of Cu and O in the lattice of pure CuO. Also, confirms the existence of Ag in CuO:Ag 5 at. %. The Ag core level spectra depict the existence of Ag in metallic (Ag^0) and ionic state (Ag^+) in CuO:Ag 5 at. %. Thus, owing to the better structural, optical, morphological and elemental results CuO:Ag can serve as potential candidates for visible light driven photodetection application.

References

[1] J.T. Chen, F. Zhang, J.Wang, G.A. Zhang, B.B. Miao, X.Y. Fan, D. Yan, P.X. Yan, J. Alloys Compd 454, 268-273 (2008); https://doi.org/10.1016/j.jallcom.2006.12.032

[2] L. Yu,G. Zhang, Y.Wu, X. Bai, D. Guo, J. Cryst. Growth 310, 3125-3130 (2008); https://doi.org/10.1016/j.jcrysgro.2008.03.026

[3] J. Zhu, H. Bi, Y. Wang, X. Wang, X. Yang, L. Lu, Mater. Lett. 61, 5236-5238 (2007); https://doi.org/10.1016/j.matlet.2007.04.037

[4] Y.K. Su, C. M.Shen, H. T.Yang, H. L.Li, H. J.Gao, Trans. Nonferrous Met. Soc. China 17, 783-786 (2007); https://doi.org/10.1016/S1003-6326(07)60174-5

[5] G.Q. Yuan, H. F.Jiang, C. Lin, S. J. Liao, J. Cryst. Growth 303, 400-406 (2007); https://doi.org/10.1016/j.jcrysgro.2006.12.047

[6] H. Zhang, S. Li, X. Ma, D. Yang, Mater. Res. Bull. 43, 1291-1296 (2008); https://doi.org/10.1016/j.materresbull.2007.05.017

[7] X. L. Tang, L. Ren, L. N.Sun, W. G.Tian, M. H.Cao, C. W. Hu, Chem. Res. Chin.Univ. 22, 547-551 (2006); https://doi.org/10.1016/S1005-9040(06)60159-1

[8] D. Keyson, D.P. Volanti, L.S. Cavalcante, A.Z. Simões, J.A. Varela, E. Longo, Mater. Res. Bull. 43, 771-775 (2008); https://doi.org/10.1016/j.materresbull.2007.03.019

[9] X. Xu, M. Zhang, J. Feng, M. Zhang, Mater. Lett. 62, 2787-2790 (2008); https://doi.org/10.1016/j.matlet.2008.01.046

[10] M. Kaur, K. P. Muthe , S. K. Despande, S. Choudhury, J. B. Singh, N. Verma, S. K. Gupta, J. V. Yakhmi, J Cryst Growth 289, 670-675 (2006); https://doi.org/10.1016/j.jcrysgro.2005.11.111

[11] J. T. Zhang, J. F. Liu, Q. Peng, X. Wang, Y. D. Li, Chem Mater 18, 867-871 (2006); https://doi.org/10.1021/cm052256f

[12] K. Yamamoto, T. Kasuga, M. Nogami, Electrochem Solid- State Lett 2, 595-596 (1999); https://doi.org/10.1149/1.1390917

[13] L. B. Chen, N. Lu, C. M. Xu, H. C. Yu, T. H. Wang, Electrochim Acta 54, 4198-4201 (2009); https://doi.org/10.1016/j.electacta.2009.02.065

[14] H. Wang, Q. Pan, J. Zhao, W. Chen, J Alloys Compd 476, 408-413 (2009); https://doi.org/10.1016/j.jallcom.2008.09.013

[15] P. Zhou, H. B. Lv, M. Yin, L. Tang, Y. L. Song, T. A. Tang, Y. Lin, J Vac SciTechnol B 26, 1030-1032 (2008); https://doi.org/10.1116/1.2927922

[16] L. Liao, Z. Zhang, B. Yan, Z. Zheng, Q. L. Bao, T. Wu, C. M. Li, Z. X. Shen, J. X. Zhang, H. Gong, J. C. Li, T. Yu, Nanotechnology 20, 085203 (2009); https://doi.org/10.1088/0957-4484/20/8/085203

[17] Priyankari Bhattacharya, Debarati Mukherjee, Surajit Dey, Sourja Ghosh, Sathi Banerj, Materials Chemistry and Physics 229, 106-116 (2019); https://doi.org/10.1016/j.matchemphys.2019.02.094

[18] Z. Zhou, Z. Zhu, F. Cui, J. Shao, H. S. Zhou, MicrochimicaActa 187, 123 (2020); https://doi.org/10.1007/s00604-019-4099-9

[19] Amir Shariffar, Haider Salman, Tanveer Ahmed Siddique, Omar Manasreh, Applied Physics A 127, 750 (2021); https://doi.org/10.1007/s00339-021-04906-x

[20] Wasan Abdulhasan, Mohammed Rasheed, Uday Nayef, Journal of Physics: Conference Series 2857, 012057 (2024); https://doi.org/10.1088/1742-6596/2857/1/012057

[21] Fateh Moëzzi, Seyyed Aliakbar Hedayati, Amir Ghadermarzi, Bulletin of Environmental Contamination and Toxicology 102, 46-51 (2019); https://doi.org/10.1007/s00128-018-2489-z

[22] Monika Patel, Sunita Mishra, Ruchi Verma, Deep Shikha, Discover Materials 2, 1 (2022); https://doi.org/10.1007/s43939-022-00022-6

[23] J. Wang, X. Cheng, P. Li, Q. Fan, D. Wu, H. Liang, Chemosphere 341, 140044 (2023); https://doi.org/10.1016/j.chemosphere.2023.140044

[24] Sagadevan Suresh, Kaushik Pal, Zaira Chowdhury, Journal of Materials Science Materials in Electronics 28 (2017); https://doi.org/10.1007/s10854-017-7083-3

[25] Sagar Vikal, Yogendra Gautam, Ashwani Kumar, Ajay Kumar, Neetu Singh, Hempal Singh, Beer Singh, Nano Express 4, 025004 (2023); https://doi.org/10.1088/2632-959X/acdc41

[26] Z. Li, Y. Xin, Z. Zhang, H. Wu, P. Wang, Sci Rep 5, 10617 (2015); https://doi.org/10.1038/srep10617

[27] Alaa Fahmy, Karam El-Nasser, Tarek Salama, Korinna Altmann, Jörg Friedrich, Tuned interactions of silver nanoparticles with ZSM-5 zeolite by adhesion-promoting poly (acrylic acid) deposited by electrospray ionization (ESI). 31, 1-16 (2017); https://doi.org/10.1080/01694243.2017.1315910